JOURNAL OF AIRCRAFT
Vol. 43, No. 3, May–June 2006

Performance and Stability Analysis of a Shrouded-Fan Unmanned Aerial Vehicle

Nicola de Divitiis*
University of Rome "La Sapienza," 00184 Rome, Italy

This paper deals with the estimation of the performance and stability for a shrouded-fan unmanned rotorcraft whose mission profile also prescribes the flight in ground effect. The not so simple estimation of the aerodynamic coefficients and of the thrust in the various situations makes the performance calculation and the stability analysis difficult tasks. This is because of the strong interaction between the fan flow and shroud that causes quite different flow structures about the airframe depending on flight conditions. A further difficulty is related to the ground effect which produces substantial modifications in the rotor thrust and aerodynamic coefficients. To evaluate performance and stability, two models have been developed. One determines the aerodynamic coefficients of the shroud, whereas the other one calculates thrust and moment of the rotors system. Both models take into account the mutual interference between fan flow and fuselage and ground effect. Performance and stability are then discussed with reference to significant flight conditions.

Nomenclature

C_l, C_m, C_n	=	hull aerodynamic-moment coefficients
$C_{l_T}, C_{m_T}, C_{n_T}$	=	rotor-moment coefficients
$C_Q \equiv C_{n_{\mathrm{Tl}}} - C_{n_{\mathrm{Tu}}}$	=	rotors system torque coefficient
$C_T \equiv -C_{Z_{\mathrm{Tl}}} - C_{Z_{\mathrm{Tu}}}$	=	rotors system thrust coefficient
C_X, C_Y, C_Z	=	hull aerodynamic-force coefficients
$C_{X_T}, C_{Y_T}, C_{Z_T}$	=	thrust-force coefficients
D	=	overall shroud diameter
d	=	rotor diameter
g	=	acceleration due to gravity
h	=	rotorcraf altitude
I_x, I_y, I_z	=	principal moments of inertia
I_{xz}	=	product of inertia
J	=	merit function
$k = V/w_D$	=	velocity parameter
L, M, N	=	hull aerodynamic-moment components
L_T, M_T, N_T	=	rotor-moment components
(p, q, r)	=	angular velocity vector in body axes
$Q = N_{\mathrm{Tl}} - N_{\mathrm{Tu}}$	=	rotors system torque
R	=	rotor radius
$S = \pi D^2/4$	=	rotorcraft reference surface
$\boldsymbol{u} \equiv (\delta_A, \delta_B, \delta_C, \delta_P)$	=	control vector
V	=	velocity modulus
$\boldsymbol{v}$	=	local fluid velocity
$\boldsymbol{v} \equiv (u, v, w)$	=	inertial velocity in body axes
$\hat{\boldsymbol{v}} \equiv \boldsymbol{v}/V = (\hat{u}, \hat{v}, \hat{w})$	=	dimensionless velocity in body axes
W	=	weight
$w_D = w_i - V \sin\alpha$	=	fluid velocity through the disk
w_i	=	induced velocity by the rotor flow on the rotor disk
X, Y, Z	=	aerodynamic-force components in body axes
X_T, Y_T, Z_T	=	thrust-force components in body axes
$\boldsymbol{x}$	=	position
x, y, z	=	inertial coordinate
x_B, y_B, z_B	=	coordinate in body axes
α, β_x	=	aerodynamic angles
α_x, β	=	angles of attack and sideslip, respectively
$\alpha_0 \equiv \pi/2 - \alpha_x$	=	axial angle of attack
$\gamma = V/\Omega R$	=	advance ratio
$\hat{\gamma}$	=	flight path angle
$\gamma_x = u/\Omega R$, $\gamma_y = v/\Omega R$, $\gamma_z = w/\Omega R$	=	dimensionless velocities
δ_A	=	lateral cyclic control, positive right
δ_B	=	longitudinal cyclic control, positive after
δ_C	=	collective control, positive up
δ_P	=	differential collective control, positive right
ε	=	ground inclination with respect to the horizontal plane
$\boldsymbol{\lambda} \equiv (\lambda_x, \lambda_y, \lambda_z)$	=	ground normal unit vector in body axes
$\lambda_i = w_i/\Omega R$	=	dimensionless induced velocity at the disk
Π_n	=	required power
ρ	=	air density
$\tau \equiv \sqrt{[1 + 4(h/R)^2]} - 2h/R$	=	ground-effect perturbative parameter
φ, ϑ, ψ	=	Euler angles
Ω	=	rotors angular velocity

Subscripts

a.c.	=	aerodynamic center
c.g.	=	vehicle center of gravity
l	=	lower rotor
u	=	upper rotor
∞	=	value calculated out-of-ground effect

Introduction

PERFORMANCE and stability calculation of a shrouded-fan unmanned aerial vehicle (UAV) is a very difficult task for various reasons. One of these is related to the intensive aerodynamic interaction between shroud and rotors[1,2] that, because of the large excursion of angle of attack and fans system induced velocity, determines quite different flow-fields about the UAV.[3–9] The simultaneous variations of angle of attack, flight speed, and the rotors induced velocity determine a wide set of flight conditions, where the aerodynamic and propulsive force and moment coefficients exhibit large variations. Furthermore the vicinity of the ground makes this study more complex because of the influence that the ground exerts on both fuselage and rotors system. Therefore, the performance and stability analysis requires an accurate vehicle aerodynamics that calculates all of

Received 21 February 2005; revision received 6 July 2005; accepted for publication 26 August 2005.

*Research Fellow, Department of Mechanics and Aeronautics, via Eudossiana, 18.

Table 1 Characteristics of the UAV

Characteristic	Value
Overall diameter, m	1.9
Rotor diameter, m	1.1
Central hub diameter, m	0.25
Maximum overall weight, N	800
Payload, N	100
Coaxial rotors	2
Power, hp	3×14
at, rpm	11,000
Rotor speed, rpm	3,000
Endurance, h	1.5
Service ceiling, m	2,000

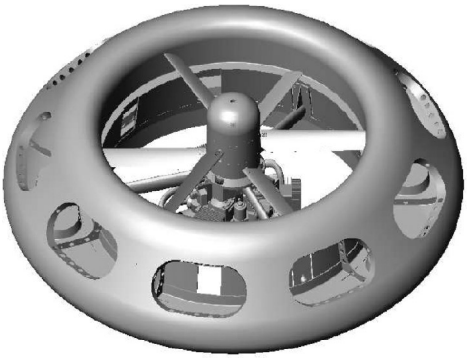

Fig. 1 Reference rotorcraft.

the aerodynamic coefficients in a wide range of angle of attack and fans working regime and an adequate model to determine the rotors force and moment in the different flight conditions. The UAV here considered is a shrouded fan made of a toroidal airframe at the center of which are placed two counter-rotating rotors driven by three two-stroke air-cooled engines (see Fig. 1), the main characteristics of which are reported in Table 1. This vehicle is similar in shape to that studied in Ref. 1 and is the result of a project jointly accomplished from the University of Rome "La Sapienza"[2] and the Polytechnic of Turin.[1] The fuselage geometry is the result of a parametric study that analyzed the lift capability of different toroidal geometries in the presence of the rotor flow. The selected fuselage cross section develops the highest lift in hovering for an assigned hull volume. The main function of the hull consists of incorporating the avionics, fuel, payload, and the possible flight-related hardware. From an aerodynamic perspective, the shroud should contain the streamlines to follow the duct and exit at an adequate velocity imposed by the exit area. Moreover the fuselage causes an intense suction force, which is produced by the inlet lip, that makes the fuselage a body with a nonnegligible lift capability. Hence the shroud generates a sizable improvement of the static thrust, which depends on the reciprocal interaction between fans system and fuselage.[5] During axial flights, the advantage in static thrust furnished by the shroud rapidly diminishes[5] as soon as the UAV increases its speed.

For what concerns the ground proximity, it is responsible for several effects. One of these is represented by the fuselage aerodynamic coefficients variations that occur in hovering. In such a situation $\varphi = \vartheta = 0$, the ground imposes a boundary condition on the aerodynamic field that symmetrically reduces the downwash of the rotors. The consequence is that the aerodynamic coefficients depend on the dimensionless height h/R, and an important loss of the fuselage lift capability is observed.[10,11] If the vehicle flies at an arbitrary inclination with respect to the ground, the interaction between rotors flow and ground alters the rotorcraft aerodynamics in such a way that the pressure distribution on the airframe depends on the height and on the vehicle attitude. Hence the aerodynamic coefficients, which are functions of the aerodynamic angles, in ground proximity also depend on the dimensionless height and on the Euler angles.

The vicinity of the ground also influences the rotors system. It has been observed that for an unducted rotor in hovering the thrust considerably increases as the height diminishes.[4–9] Furthermore the attitude modifies rotor actions[12] so that in ground effect thrust and torque depend on the Euler angles. As a result, the attitude can play an important role for the determination of the flying qualities depending on the height. Also the ground inclination with respect to the horizon is of great importance in ground effect. This can be the case of a rotorcraft that approaches a ship flight deck,[12,13] whose inclination influences the vehicle aerodynamics and rotors thrust and moment.[12] The deck oscillations caused by the ship attitude motion determine unsteady thrust and aerodynamic force and moment, which influence the rotorcraft dynamics. Another source of the significant variations of the performance and stability in ground effect is a nonzero flight-path angle, which determines incremental aerodynamic force and thrust.[14] This can happen during maneuvers that are used to avoid collisions with low obstacles. The aforementioned effects are more pronounced at low height where the ground effect is more intense and can determine sizable variations of trim controls and rotorcraft stability margin.

Although several studies on the mutual interference between hull aerodynamics, rotor flow, and ground effect[12,14–17] were developed, to the author's knowledge a general analysis of these phenomena in terms of rotorcraft flight dynamics has not received due attention. Therefore, the objective of the present work is to develop an accurate mathematical model that can be adopted for the analysis of the performance and flying qualities of the UAV.

In the present study two models are proposed. The first one calculates the shroud aerodynamic coefficients, whereas the second one determines the rotors force and moment through the blade-element theory. Both models account for the mutual interaction between hull and rotors and the ground proximity. The aerodynamic model exhibits free parameters that have to be identified. These models allow the forces and moments to be accurately formulated and the performance and flying quality to be interpreted. Obtained results are compared with data reported in the literature, and finally a detailed analysis of the performance characteristics and flying qualities of the vehicle is carried out.

Aerodynamic Model

A method to calculate the aerodynamic force and moment on the UAV shroud configuration is now presented. This procedure, based on physical considerations, takes into account the reciprocal influence between rotors flow and fuselage and the possible presence of the ground. First, it is necessary to establish the flow structure about the airframe that in turn directly depends on the rotors system working regime. Figure 2 shows the regions of the four characteristic working regimes in terms of the induced and axial velocities.[3–6] In this study the vehicle aerodynamics is modeled according to the normal working state, which corresponds to situations where the induced velocity is sufficiently high with respect to the axial velocity $V \sin\alpha$. In this situation the rotors flow enters from the top of the rotorcraft, the air is then ejected towards the bottom, and the power is transferred from the rotors to the air. The other working regimes, such as the windmill-brake state, the turbulent wake state, and the vortex ring state are not studied in the present analysis because they are considered to be off-design situations that correspond to

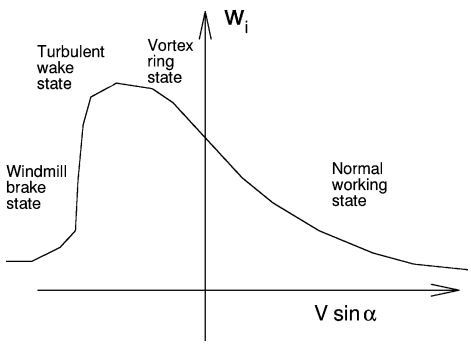

Fig. 2 Rotor working regimes.

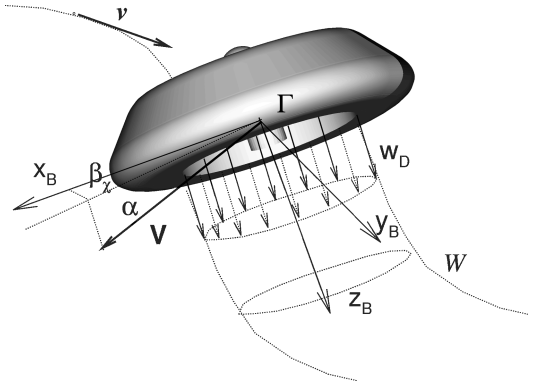

Fig. 3 Vehicle aerodynamics in normal working state out of ground effect.

more complicated flow conditions that strongly reduce the hull lift capability.

Figure 3 shows the rotorcraft in normal working state, out-of-ground effect. The rotors flow and the external stream are separated by the wake W, which originates from the separation line Γ that is assumed to be equal to the circumference of the exit area. Because of the axial symmetry around z_B, the sideslip angle does not influence the shroud aerodynamics. Aerodynamic force $\boldsymbol{F}_A$ and moment $\boldsymbol{M}_A$ lie on the plane $z_B - V$, which is defined by z_B and $\boldsymbol{v}$. This plane defines a reference frame (x_v, y_v, z_v) whose axes are oriented so that $z_v \equiv z_B$, and y_v is normal to both z_v and $\boldsymbol{v}$, whereas x_v is perpendicular to both y_v and z_v. In this frame $\boldsymbol{F}_A$ and $\boldsymbol{M}_A$ are expressed as

$$\boldsymbol{F}_A = (\bar{X}, 0, \bar{Z}), \qquad \boldsymbol{Q}_A = (0, \bar{M}, 0) \tag{1}$$

where all of the components are independent on the sideslip angle. Because of the axial symmetry, instead of using the angle of attack α_x and sideslip β, it is convenient to introduce different aerodynamic angles, that is, α and β_x, which are defined as follows[1,2]:

$$\begin{bmatrix} u \\ v \\ w \end{bmatrix} \equiv V \begin{bmatrix} \hat{u} \\ \hat{v} \\ \hat{w} \end{bmatrix} = V \begin{bmatrix} \cos\alpha\cos\beta_x \\ \cos\alpha\sin\beta_x \\ \sin\alpha \end{bmatrix} \tag{2}$$

The components in body axes of $\boldsymbol{F}_A$ and $\boldsymbol{Q}_A$ in terms of β_x are expressed as

$$\begin{aligned} X &= \bar{X}\cos\beta_x, \qquad Y = \bar{X}\sin\beta_x, \qquad Z = \bar{Z} \\ L &= -\bar{M}\sin\beta_x, \qquad M = \bar{M}\cos\beta_x, \qquad N = 0 \end{aligned} \tag{3}$$

The hull aerodynamics is strongly influenced by the rotors flow. In this model an equivalent actuator disk is placed in the mid of the two rotors, whose induced velocity w_i coincides with that produced by the rotors at the actuator disk plane. Therefore, the rotor flow is supposed to be generated by an uniform layer of doublets with a proper value of w_i. The induced velocity, which in turn represents the effect of the collective pitch on the vehicle aerodynamics, is determined by means of the rotor model described later in the dedicated section. Nonuniform distributions of w_i on the disk plane, caused by the cyclic pitch, are neglected.

To derive the analytical expressions of the aerodynamic force and moment coefficients, the rotorcraft is considered in a steady-state potential flow. Then, the flow velocity in a point $\boldsymbol{x}$ of the space is given by[18]

$$\boldsymbol{v}(\boldsymbol{x}) = \frac{\partial \boldsymbol{v}}{\partial \boldsymbol{v}}\boldsymbol{v} + \frac{\partial \boldsymbol{v}}{\partial w_D} w_D \tag{4}$$

where $\partial\boldsymbol{v}/\partial\boldsymbol{v}$ and $\partial\boldsymbol{v}/\partial w_D$ are influence matrices. In Eq. (4) the first term gives the effect of the flight velocity on the vehicle aerodynamics, whereas the second one provides the contribution caused by the rotors flow. Force and moment depend on the local pressure distribution, which is related to the square of the local velocity

$$\begin{aligned} \boldsymbol{v}^2 &= (\mu_1\cos^2\alpha + \mu_2\sin 2\alpha + \mu_3\sin^2\alpha)V^2 \\ &\quad + 2V w_D(\chi_1\cos\alpha + \chi_2\sin\alpha) + g^2 w_D^2 \end{aligned} \tag{5}$$

by means of the Bernoulli theorem, where μ_i and χ_i are functions of the position through $\partial\boldsymbol{v}/\partial\boldsymbol{v}$ and $\partial\boldsymbol{v}/\partial w_D$. Because of the symmetry around z_B, the pressure does not depend on the sideslip angle. The aerodynamic force and moment are then expressed as surface integrals of the local pressure

$$\boldsymbol{F}_A = \iint p\boldsymbol{n}\,\mathrm{d}S, \qquad \boldsymbol{Q}_A = \iint (\boldsymbol{r} - \boldsymbol{r}_{\mathrm{c.g.}}) \times \boldsymbol{n} p\,\mathrm{d}S \tag{6}$$

Substituting Eq. (5) into Eqs. (6), one obtains the aerodynamic coefficients on the plane $z_v - V$ in terms of k and α:

$$\begin{aligned} \bar{C}_X(\alpha, k) &= F_1(k,\alpha)X_1\sin 2\alpha + F_2(k,\alpha)X_2\cos\alpha \\ \bar{C}_Z(\alpha, k) &= F_0(k,\alpha)Z_0 + F_1(k)Z_1\sin\alpha \\ &\quad + F_2(k,\alpha)\left(Z_{21}\cos^2\alpha + Z_{22}\sin^2\alpha\right) \\ \bar{C}_m(\alpha, k) &= F_1(k,\alpha)M_1\sin 2\alpha + F_2(k,\alpha)M_2\cos\alpha \end{aligned} \tag{7}$$

that are defined by means of

$$\boldsymbol{F}_A = \tfrac{1}{2}\rho V_f^2 S(\bar{C}_X, 0, \bar{C}_Z), \qquad \boldsymbol{Q}_A = \tfrac{1}{2}\rho V_f^2 SD(0, \bar{C}_m, 0) \tag{8}$$

where

$$V_f = \sqrt{u^2 + v^2 + (w - w_i)^2} \equiv \sqrt{V^2\cos^2\alpha + w_D^2} \tag{9}$$

while the functions F_0, F_1, and F_2 are given by

$$\begin{aligned} F_0(k,\alpha) &= \frac{1}{k^2\cos^2\alpha + 1}, \qquad F_1(k,\alpha) = \frac{k}{k^2\cos^2\alpha + 1} \\ F_2(k,\alpha) &= \frac{k^2}{k^2\cos^2\alpha + 1} \end{aligned} \tag{10}$$

The aerodynamic coefficients in body axes are then obtained as the projection of Eqs. (7) in body frame, that is,

$$\begin{aligned} C_X &= \bar{C}_X\cos\beta_x, \qquad C_Y = \bar{C}_X\sin\beta_x, \qquad C_Z = \bar{C}_Z \\ C_l &= -\bar{C}_m\sin\beta_x, \qquad C_m = \bar{C}_m\cos\beta_x, \qquad C_n = 0 \end{aligned} \tag{11}$$

The angular velocity is taken into account by rotational derivatives, the expressions of which are[18]

$$\begin{aligned} C_{X_p} &= 0, \qquad C_{X_q} = M_{33}\sin\alpha, \qquad C_{X_r} = -M_{11}\cos\alpha\sin\beta_x \\ C_{Y_p} &= -M_{33}\sin\alpha, \qquad C_{Y_q} = 0, \qquad C_{Y_r} = M_{11}\cos\alpha\cos\beta_x \\ C_{Z_p} &= M_{11}\cos\alpha\sin\beta_x, \qquad C_{Z_q} = -M_{11}\cos\alpha\cos\beta_x \\ C_{Z_r} &= 0, \qquad C_{l_p} = K_{12}\sin\alpha, \qquad C_{l_q} = (K_{33} - K_{11})\sin\alpha \\ C_{l_r} &= (K_{33} - K_{11})\cos\alpha\sin\beta_x - K_{12}\cos\alpha\cos\beta_x \\ C_{m_p} &= (K_{11} - K_{33})\sin\alpha \qquad C_{m_q} = K_{12}\sin\alpha \\ C_{m_r} &= (K_{11} - K_{33})\cos\alpha\cos\beta_x - K_{12}\cos\alpha\sin\beta_x \end{aligned} \tag{12}$$

where

$$\begin{aligned} M_{ij} &= M_{ij0}F_0(k,\alpha) + M_{ij1}F_1(k,\alpha) \\ K_{ij} &= K_{ij0}F_0(k,\alpha) + K_{ij1}F_1(k,\alpha) \end{aligned} \tag{13}$$

Equations (12) represent the expressions of the rotational derivatives of a body that exhibits an axial symmetry around z_B. The quantities M_i, X_i, Z_i appearing in Eqs. (7) and Z_{ij}, M_{ij0}, M_{ij1}, K_{ij0}, and K_{ij1}

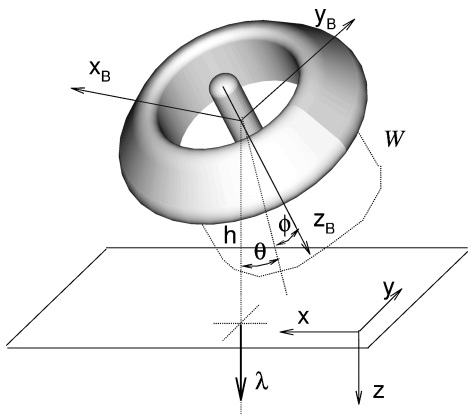

Fig. 4 Vehicle aerodynamics in ground effect.

appearing in Eqs. (12) and (13) are free parameters that depend on the vehicle geometry.

In ground effect, the rotor downwash is limited by the ground surface, so that the velocity field about the airframe is modified with respect to Eq. (4). To study this situation, consider now Fig. 4, where the rotorcraft in close proximity to the flat ground is analyzed. The wake W is considered to be a rigid cylinder whose length is assigned in advance in such a way that it does not intersect the ground plane. The ground inclination with respect to the rotorcraft is represented by the unit vector

$$\boldsymbol{\lambda} \equiv (\lambda_x, \lambda_y, \lambda_z) = (-\sin\vartheta, \sin\varphi\cos\vartheta, \cos\varphi\cos\vartheta) \tag{14}$$

which is the normal unit vector of the ground plane in body axes. The presence of the ground is simulated by placing a specular image of the rotorcraft at an equal distance below the ground plane. According to the potential flow theory,[18] the local velocity is the sum of those induced by the vehicle and by its mirror image, that is,

$$\boldsymbol{v}(\boldsymbol{x}) = \boldsymbol{v}_\infty(\boldsymbol{x}) + \frac{\partial \boldsymbol{v}}{\partial\{\boldsymbol{\lambda} w_D\}} w_D \boldsymbol{\lambda} + \frac{\partial^2 \boldsymbol{v}}{\partial \boldsymbol{\lambda} \partial \boldsymbol{v}} \boldsymbol{\lambda} \boldsymbol{v} \tag{15}$$

The first addend is the local velocity induced by the entire rotorcraft, whereas the second and the third ones provide, respectively, the interaction between rotors flow and ground plane and the influence that the ground exerts on the fuselage. The pressure about the airframe is then altered by the vicinity of the ground, so that the aerodynamic coefficients also depend on height and attitude. Now, to obtain the expressions of the force and moment in ground effect, the kinetic energy of the stream T is considered. Following Ref. 18, T is a definite positive quadratic form that is a function of $\boldsymbol{v}$, w_D, and $\boldsymbol{\lambda}$. To determine the expression of T, consider now two sets of flight conditions. The first of these corresponds to horizontal flights $[\boldsymbol{\lambda} = (0, 0, 1)]$, where $\boldsymbol{v}$ describes a circular cone about z_B, whereas the second one consists of axial flights $[\boldsymbol{v} = (0, 0, V)]$ with $\boldsymbol{\lambda}$, which makes a circular cone about z_B. In both cases, because of the axial symmetry about z_B the kinetic energy must remain unaltered. As a result, the kinetic energy of the stream can be written in the form

$$T = f_1(u^2 + v^2) + f_2 w^2 + f_3 w_D(u\lambda_x + v\lambda_y) + f_4 w_D w \lambda_z \tag{16}$$

where f_1, f_2, f_3, and f_4 are functions of h/R that, according to Ref. 19, are written in terms of h/R by means of the perturbative parameter τ, that is,

$$f_k = \sum_{m=1}^{3} f_{km} \tau^m \qquad (k = 1, 2, 3, 4) \tag{17}$$

The shroud aerodynamic force and moment increments developed in-ground effect are then expressed using the Lagrange equations method[18]

$$\Delta \boldsymbol{F} \equiv (\Delta X, \Delta Y, \Delta Z) = -\frac{\partial}{\partial t}\frac{\partial T}{\partial \boldsymbol{v}} - \frac{\partial}{\partial h}\frac{\partial T}{\partial \boldsymbol{v}} V \sin\hat{\gamma}$$

$$\Delta \boldsymbol{Q} \equiv (\Delta L, \Delta M, \Delta N) = -\boldsymbol{v} \times \frac{\partial T}{\partial \boldsymbol{v}} + \boldsymbol{r}_{\mathrm{AG}} \times \Delta \boldsymbol{F} \tag{18}$$

where $\boldsymbol{r}_{\mathrm{AG}} \equiv \boldsymbol{r}_{\mathrm{a.c.}} - \boldsymbol{r}_{\mathrm{c.g.}} = (x_{\mathrm{AG}}, y_{\mathrm{AG}}, 0)$ is the position of the aerodynamic center with respect to c.g., which varies in ground effect. Out of ground effect it is assumed that $\boldsymbol{r}_{\mathrm{a.c.}} = \boldsymbol{r}_{\mathrm{c.g.}}$, whereas close to the ground $\boldsymbol{r}_{\mathrm{a.c.}}$ depends upon the flight conditions. Because the yaw moment must be equal to zero in all of the situations, the projection along z_B of $\boldsymbol{r}_{\mathrm{AG}} \times \Delta \boldsymbol{F}$ must be identically equal to zero. The consequence is that $\boldsymbol{r}_{\mathrm{AG}}$ assumes the form

$$\boldsymbol{r}_{\mathrm{AG}}/R = \zeta(\Delta X/Z_\infty, \Delta Y/Z_\infty, 0) \tag{19}$$

where ζ is a quantity depending on h/R, which is expressed through τ

$$\zeta = \sum_{k=0}^{3} \chi_k \tau^k \tag{20}$$

Substituting Eq. (16) into Eqs. (18), one obtains the incremental force and moment in ground effect

$$\begin{aligned}
\Delta X &= -(2\dot{f}_1 u + \dot{f}_3 w_D \lambda_x) - \left(2f_{1_h} u + f_{3_h} w_D \lambda_x\right) V \sin\hat{\gamma} \\
\Delta Y &= -(2\dot{f}_1 v + \dot{f}_3 w_D \lambda_y) - \left(2f_{1_h} v + f_{3_h} w_D \lambda_y\right) V \sin\hat{\gamma} \\
\Delta Z &= -(2\dot{f}_2 w + \dot{f}_4 w_D \lambda_z) - \left(2f_{2_h} w + f_{4_h} w_D \lambda_z\right) V \sin\hat{\gamma} \qquad (21) \\
\Delta L &= -2(f_2 - f_1) vw - f_3 w_D \lambda_z v - \chi R\big[(2\dot{f}_1 v + \dot{f}_3 w_D \lambda_y) \\
&\quad + \left(2f_{1_h} v + f_{3_h} w_D \lambda_y\right) V \sin\hat{\gamma}\big] \\
\Delta M &= 2(f_2 - f_1) uw + f_3 w_D \lambda_z u + \chi R\big[(2\dot{f}_1 u + \dot{f}_3 w_D \lambda_x) \\
&\quad + \left(2f_{1_h} u + f_{3_h} w_D \lambda_x\right) V \sin\hat{\gamma}\big] \\
\Delta N &= 0 \qquad (22)
\end{aligned}$$

where the quantities $\dot{f}_k$ and f_h are

$$\dot{f}_k = \dot{f}_{\mathrm{kv}} V + \dot{f}_{\mathrm{kw}_D} w_D, \qquad f_{k_h} = f_{\mathrm{kv}} V + f_{\mathrm{kw}_D} w_D \tag{23}$$

Following the classical theory of the lifting bodies, both $\dot{f}_k$ and f_h are proportional to the circulation around the hull. In particular, $\dot{f}_k$ is the time derivative of f_k, which is caused by the wake, while f_{k_h} is the derivative of f_k with respect to h, which is related to the sink rate. Accounting for the variations of ζ and f_k, the aerodynamic-force coefficients can be written in the form

$$\begin{aligned}
\Delta C_x &= \sum_{m=0}^{2}\sum_{n=1}^{3} F_m(k,\alpha)\tau^n[(A_{\mathrm{mn}}\hat{u} + B_{\mathrm{mn}}\lambda_x) \\
&\quad + (C_{\mathrm{mn}}\hat{u} + D_{\mathrm{mn}}\lambda_x)\sin\hat{\gamma}] \\
\Delta C_y &= \sum_{m=0}^{2}\sum_{n=1}^{3} F_m(k,\alpha)\tau^n[(A_{\mathrm{mn}}\hat{v} + B_{\mathrm{mn}}\lambda_y) \\
&\quad + (C_{\mathrm{mn}}\hat{v} + D_{\mathrm{mn}}\lambda_y)\sin\hat{\gamma}] \\
\Delta C_z &= \sum_{m=0}^{2}\sum_{n=1}^{3} F_m(k,\alpha)\tau^n[(E_{\mathrm{mn}}\hat{w} + G_{\mathrm{mn}}\lambda_z) \\
&\quad + (H_{\mathrm{mn}}\hat{w} + L_{\mathrm{mn}}\lambda_z)\sin\hat{\gamma}] \qquad (24)
\end{aligned}$$

whereas the aerodynamic-moment coefficients are

$$\begin{aligned}
\Delta C_l &= \sum_{m=0}^{2}\sum_{n=1}^{3} F_m(k,\alpha)\tau^n[(N_{\mathrm{mn}}\hat{v} + P_{\mathrm{mn}}\hat{v}\hat{w} + Q_{\mathrm{mn}}\lambda_z\hat{v} + R_{\mathrm{mn}}\lambda_y) \\
&\quad + (S_{\mathrm{mn}}\hat{v} + T_{\mathrm{mn}}\hat{v}\hat{w} + U_{\mathrm{mn}}\lambda_z\hat{v} + V_{\mathrm{mn}}\lambda_y)\sin\hat{\gamma}] \\
\Delta C_m &= -\sum_{m=0}^{2}\sum_{n=1}^{3} F_m(k,\alpha)\tau^n[(N_{\mathrm{mn}}\hat{u} + P_{\mathrm{mn}}\hat{u}\hat{w} + Q_{\mathrm{mn}}\lambda_z\hat{u} \\
&\quad + R_{\mathrm{mn}}\lambda_x) + (S_{\mathrm{mn}}\hat{u} + T_{\mathrm{mn}}\hat{u}\hat{w} + U_{\mathrm{mn}}\lambda_z\hat{u} + V_{\mathrm{mn}}\lambda_x)\sin\hat{\gamma}] \\
\Delta C_n &= 0 \qquad (25)
\end{aligned}$$

In Eqs. (24) and (25) the coefficients A_{mn}, B_{mn}, C_{mn}, D_{mn}, E_{mn}, G_{mn}, H_{mn}, L_{mn}, N_{mn}, P_{mn}, Q_{mn}, R_{mn}, S_{mn}, T_{mn}, U_{mn}, and V_{mn} are the free parameters of the aerodynamic model in ground effect. Because for $k \to 0$, $\Delta C_x = \Delta C_y = \Delta C_l = \Delta C_m$ do not depend on the aerodynamic angles, one has $A_{0n} = C_{0n} = E_{0n} = H_{0n} = N_{0n} = P_{0n} = Q_{0n} = S_{0n} = T_{0n} = U_{0n} = 0$. The terms with $\sin\hat{\gamma}$ yield the influence of the sink rate on the shroud aerodynamics. A nonzero sink rate determines an unsteady ground effect that modifies the aerodynamic coefficients according to the Bernoulli theorem

$$\frac{\partial\phi}{\partial t} + \frac{\boldsymbol{v}\cdot\boldsymbol{v}}{2} + \frac{p}{\rho} = \text{const} \tag{26}$$

where $\partial\phi/\partial t = \partial\phi/\partial h\dot{h} \equiv \partial\phi/\partial h V \sin\hat{\gamma}$ is the unsteady term that produces the dynamic ground effect. As for the influence of the spin rate, Eqs. (12) are considered to be valid also in ground effect.

Rotors System Model

The rotors actions provide lift force and control moments to manage rotorcraft attitude. Pitch and roll are controlled through longitudinal δ_B and lateral δ_A variations of blade pitch, whereas the yaw control is carried out by means of differential variation δ_P of the collective pitch on both rotors, whose angular velocity is kept constant by a rpm governor. The blade pitch is controlled by a mechanism consisting of two independent swashplates, each driven by three actuators.

Thrust forces and moments developed by the rotors are given by the equations[6]

$$(X_T, Y_T, Z_T) = -\pi\rho\Omega^2 R^4\left(C_{x_T}, C_{y_T}, C_{z_T}\right)$$

$$(L_T, M_T, N_T) = \pi\rho\Omega^2 R^5\left(C_{l_T}, C_{m_T}, C_{n_T}\right) \tag{27}$$

where $C_{x_T}, C_{y_T}, C_{z_T}$ and $C_{l_T}, C_{m_T}, C_{n_T}$ are, respectively, thrust and torque coefficients. They are obtained with the blade-element theory, which calculates thrust and moment through analytical integration of the aerodynamic load along the blade span assuming steady-state aerodynamics,[1] where the effects of the blade-tip losses and the mutual influence between the two rotors are neglected. The determination of the rotors regime is made by imposing that the thrust coefficient $C_{z_T}(\gamma_x, \gamma_y, \gamma_z)$, calculated with the blade-element theory, is equal to that obtained by the actuator disk theory,[20] that is

$$C_{z_T a} = 2\lambda_i\sqrt{\gamma_z^2 + \lambda_i^2 - 2\gamma_z\lambda_i\sin\alpha} \tag{28}$$

where

$$\gamma_x = (u + u_s)/\Omega R, \qquad \gamma_y = (v + v_s)/\Omega R$$

$$\gamma_z = (w + w_s)/\Omega R, \qquad \lambda_i = w_i/\Omega R \tag{29}$$

and

$$(u_s, v_s, w_s) = \frac{\partial\boldsymbol{v}}{\partial\boldsymbol{v}}\cdot\boldsymbol{v} \tag{30}$$

is the velocity induced by the shroud at the center of the actuator disk plane. As a result, one obtains the following equation:

$$C_{z_T}(\gamma_x, \gamma_y, \gamma_z) = 2\lambda_i\sqrt{\gamma_z^2 + \lambda_i^2 - 2\gamma_z\lambda_i\sin\alpha} \tag{31}$$

the solution of which gives the dimensionless induced velocity λ_i and the corresponding thrust coefficient. To take into account the ground effect, the ground is modeled by means of the mirror image of the entire rotorcraft. Equation (31) is still considered valid even though (u_s, v_s, w_s) now accounts for the induced velocity of the mirror image calculated in the origin of the actuator disk plane, that is,

$$(u_s, v_s, w_s) = \frac{\partial\boldsymbol{v}}{\partial\boldsymbol{v}}\cdot\boldsymbol{v} + \frac{\partial\boldsymbol{v}}{\partial\boldsymbol{\lambda} w_D}w_D\boldsymbol{\lambda} + \frac{\partial^2\boldsymbol{v}}{\partial\boldsymbol{\lambda}\partial\boldsymbol{v}}\boldsymbol{\lambda}\boldsymbol{v} \tag{32}$$

A nonzero sink rate determines an unsteady ground effect for the rotors system, then following the Bernoulli theorem, the pressure distribution along each blade is augmented by the quantity

$$\Delta p = -\rho\frac{\partial\phi}{\partial h}V\sin\hat{\gamma} \tag{33}$$

that expresses the pressure increment caused by the dynamic ground effect.

Equations of Motion

A full nonlinear six-degrees-of-freedom model of the vehicle is now defined. Following Etkin,[21] the equations of motion for the rotorcraft are written as follows:

$$\dot{u} = g[(X_T + X)/W] - g\sin\vartheta - qw + rv$$

$$\dot{v} = g[(Y_T + Y)/W] + g\cos\vartheta\sin\varphi - ru + pw$$

$$\dot{w} = g[(Z_T + Z)/W] + g\cos\vartheta\cos\varphi - pv + qu$$

$$\dot{\varphi} = p + \sin\varphi\tan\vartheta q + \cos\varphi\tan\vartheta r$$

$$\dot{\vartheta} = \cos\varphi q - \sin\varphi r$$

$$\dot{\psi} = \sin\varphi\sec\vartheta q + \cos\varphi\sec\vartheta r$$

$$\dot{p} = \{[I_{xz}pq + (I_y - I_z)qr + L + L_T]I_z + [-I_{xz}qr + (I_x - I_y)pq + N + N_T]I_{xz}\}\Big/\left(I_xI_z - I_{xz}^2\right)$$

$$\dot{q} = \left[I_{xz}(r^2 - p^2) + (I_z - I_x)pr + M + M_T\right]\Big/I_y$$

$$\dot{r} = \{[-I_{xz}qr + (I_x - I_y)pq + N + N_T]I_x + [I_{xz}pq + (I_y - I_z)qr + L + L_T]I_{xz}\}\Big/\left(I_xI_z - I_{xz}^2\right)$$

$$\dot{x} = (\cos\vartheta\cos\psi)u + (\sin\varphi\sin\vartheta\cos\psi - \cos\varphi\sin\psi)v + (\cos\varphi\sin\vartheta\cos\psi + \sin\varphi\sin\psi)w$$

$$\dot{y} = (\cos\vartheta\sin\psi)u + (\sin\varphi\sin\vartheta\sin\psi + \cos\varphi\cos\psi)v + (\cos\varphi\sin\vartheta\sin\psi - \sin\varphi\cos\psi)w$$

$$\dot{z} = (-\sin\vartheta)u + (\sin\varphi\cos\vartheta)v + (\cos\varphi\cos\vartheta)w \tag{34}$$

Both the coaxial rotors cause moments that are transmitted to the fuselage. Because the rigid rotors have the same moments of inertia with respect to the rotation axis, their gyroscopic effects balance each other and therefore do not appear in the rigid-body moment equations.

Identification of the Aerodynamic Model Parameters

This section describes the identification procedure for the free parameters of the aerodynamic model. The algorithm consists of an optimization method, based on the least-square procedure, which is represented by the problem

$$J = \sum_k[(C_k)_{\text{CFD}} - C_k]^2 = \min \tag{35}$$

where C_k is the generic aerodynamic coefficient calculated with the proposed model, whereas $(C_k)_{\text{CFD}}$ is the same coefficient computed by computational-fluid-dynamics (CFD) simulations. These simulations are obtained using VSAERO by Analytical Methods, Inc.,[22] which is a code based on a boundary integral formulation. The code accounts for the aforementioned effects such as the interference between fan flow and airframe, the ground effect, and the presence of the separated flows enclosed by the wake.

The design variables of the problem given by Eq. (35) are defined as the arguments of J, which are the aerodynamic model free parameters.

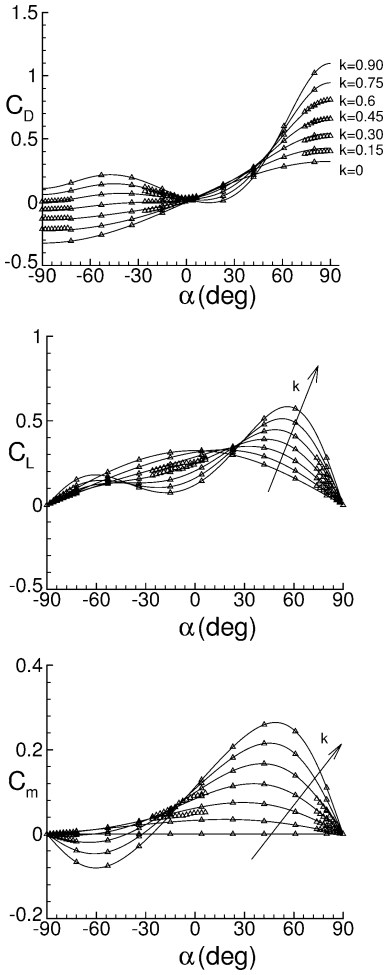

Fig. 5 Aerodynamic coefficients out of ground effect.

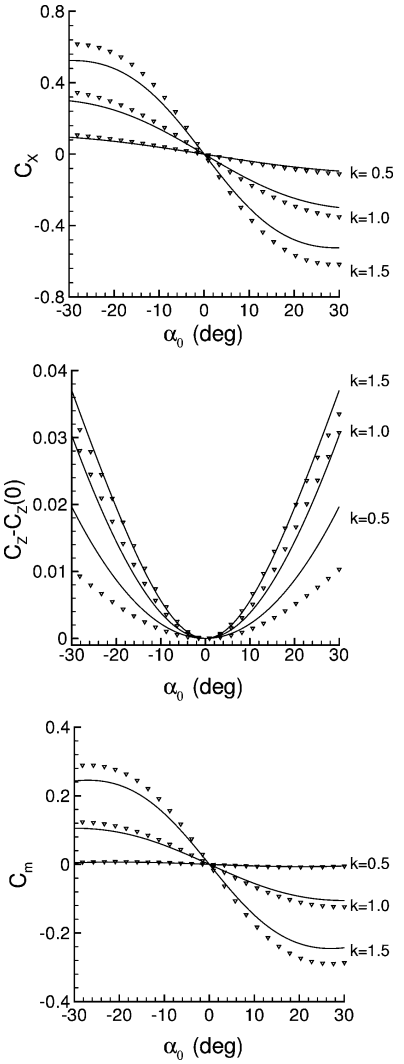

Fig. 6 Aerodynamic coefficients out of ground effect: ——, present data; and symbols are from Ref. 23.

The free parameters of the model out of ground effect are determined first. They are the coefficients of the Eqs. (7) and (13), which are identified through several CFD calculations. Once the simulations are carried out, the quantities $\partial \boldsymbol{v}/\partial \boldsymbol{v}$ and $\partial \boldsymbol{v}/\partial w_D$ are also determined. The results are shown in Fig. 5, which reports drag, lift and pitch-moment coefficients, where the continuous lines and the solid symbols are, respectively, the results calculated by the model and the data obtained by VSAERO.

For what concerns the ground effect, the free parameters are the coefficients of Eqs. (24) and (25). To assess the simultaneous influence of α, β_x, φ, ϑ, h/R, and k on the vehicle aerodynamics in ground effect, a large number of CFD simulations is made with VSAERO, for several flight conditions. The model free parameters are then calculated using the aforementioned minimization algorithm, so that also the influence functions $\partial \boldsymbol{v}/\partial \boldsymbol{\lambda} w_D$, $\partial^2 \boldsymbol{v}/\partial \boldsymbol{\lambda} \partial \boldsymbol{v}$, and $\partial \phi/\partial h$ are evaluated.

Validation of the Models

To validate the proposed models, the present results are compared with some existing data in the literature.

In Fig. 6 the aerodynamic coefficients in body axes in terms of α_0 are depicted. The present results (continuous lines) are compared with those from Ref. 23 (solid symbols). This latter model is based upon Fourier expansion of the vorticity distribution that accounts for the effects of camber, taper, and thickness. These data are determined by combining all of these effects to obtain a similar toroidal fuselage to the shroud here studied. Some discrepancy is apparent, especially for C_z when k tends to zero, that could be caused by the difference between the two geometries. In spite of that, the present results can be considered somewhat comparable with those obtained using the model of Ref. 23.

As for the ground effect, it is known that for a platform in the presence of a lifting jet[10] the hull exhibits a substantial lift reduction[10,11] that becomes more influent as the fuselage approaches to the ground. In the case of hovering ($V = \varphi = \vartheta = 0$), it can be shown through the Buckingham theorem that, for given thrust and hull geometry, the dimensionless parameters which describe the lift loss phenomenon are $\Delta Z/Z_\infty$ and $h/(D-d)$ (Refs. 10 and 11). Figure 7a shows the present results (continuous line) in comparison with the data from Refs. 10 and 11 (dashed line and solid symbols, respectively), which are static measurements of the lift losses in ground effect for a circular platform. The present data are referred to a toroidal fuselage, while Refs. 10 and 11 deal with circular planforms with a centrally located lifting jet. Nevertheless, the obtained results are qualitatively in good agreement with the those of Refs. 10 and 11.

The aerodynamic coefficients in ground effect also depend on the vehicle attitude and sink rate. Then, Figs. 7b–7d show the increments of the longitudinal aerodynamic coefficients (continuous lines), calculated at $\varphi = 0, k = 0$ for various h/R, while Fig. 7e gives the derivative $\partial C_z/\partial \gamma$ at $\alpha = \pi/2$, vs k, where each curve represents a given h/R. The results are represented together with those of a rigid vortex ring in the vicinity of a wall (solid symbols), where the vortex geometry is assumed to be equal to the circumference defined by the centers of the shroud cross sections, whereas the vortex circulation is selected in such a way that the induced velocity at the center of the vortex ring is equal to w_i. As well as in the cases of the hull and rotors system, the wall is simulated by means of the vortex ring mirror image, where the induced velocity on each vortex element is calculated by means of the Biot–Savart law, whereas

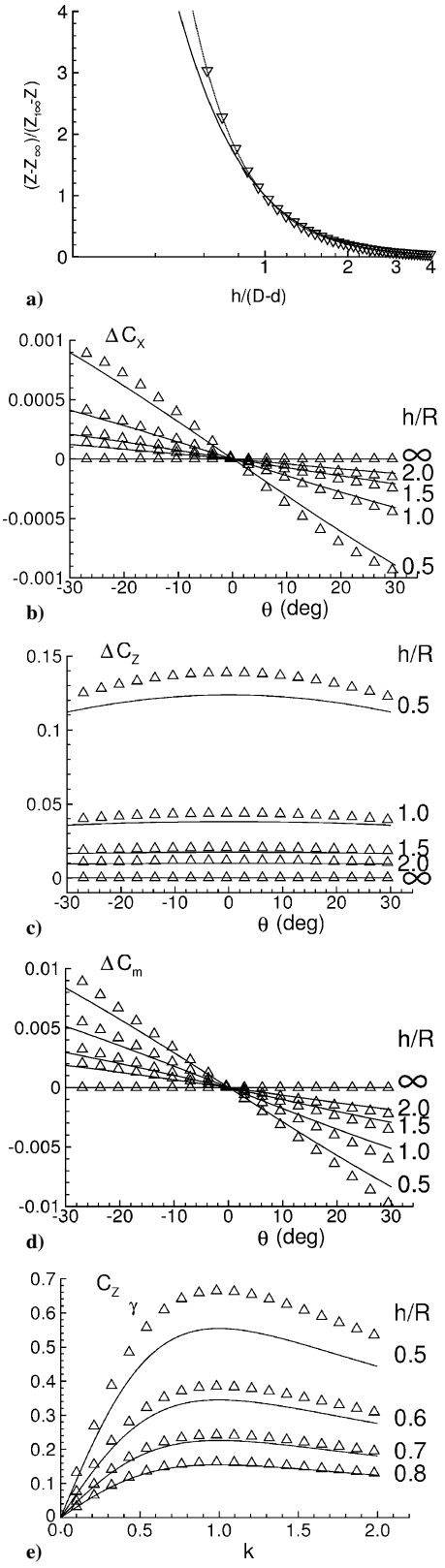

Fig. 7 Aerodynamic coefficients in ground effect.

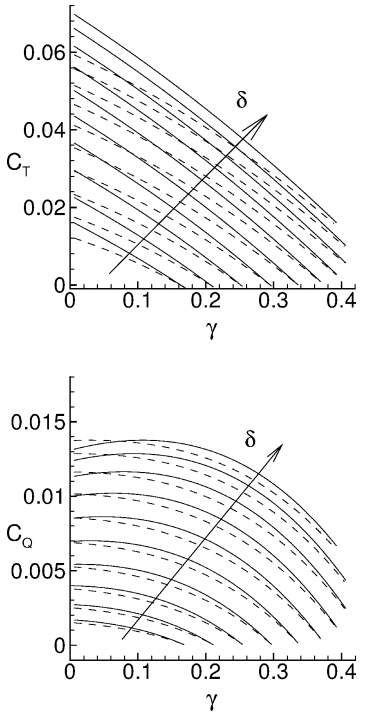

Fig. 8 Thrust and torque coefficients in axial flight out of ground effect: – – – and ——, respectively, for free and shrouded rotors.

the corresponding action is determined using the Kutta–Joukowsky theorem. Some disagreement is evident, as a result of the geometrical differences between toroidal fuselage and vortex ring, which becomes more significant as h/R goes to zero. Nevertheless, the obtained results seem to be in adequate agreement with those of the vortex ring. Because of the symmetry around z_B, ΔC_x and ΔC_m are odd functions, while ΔC_z is an even function of ϑ. ΔC_z varies in accordance with Fig. 7c and presents minor variations with ϑ but for $h/R \to 0$, while C_m exhibits a negative slope whose absolute value increases as h/R approaches zero. This last characteristic corresponds to a positive contribution to the rotorcraft stability in ground effect. The plot of Fig. 7e, which illustrates the effect of the sink rate on the hull aerodynamics, shows the derivative $\partial C_z/\partial\gamma$ in terms of k. A negative flight-path angle (positive sink rate) produces a negative variation of C_z that corresponds to a an increment of the shroud lift coefficient. For each curve, $\partial C_z/\partial\gamma$ exhibits its maximum value at about $k = 1$. As for the lateral coefficients, because of the hull symmetry, when ϑ is changed with φ, then C_x, C_m are changed in C_y and $-C_l$, respectively.

For what concerns the rotors model, various calculations have been carried out. Figure 8 gives C_T and C_Q of the rotors system in axial flight with (continuous lines) and without (dashed lines) shroud in terms of the advance ratio for several collective pitch. In both cases, the rotors system exhibits the behavior of a propeller in axial flight, whereas the presence of the shroud produces sizable variations in the thrust. For each collective pitch, at $\gamma = 0$ (static case), the fuselage generates a thrust gain of about 25% with respect to the unshrouded rotor, whereas, as soon as the advance ratio increases, a more limited thrust gain is observed. As for the torque coefficient, minor variations are observed. This results are in accordance with Refs. 3 and 5, where similar configurations of ducted propeller are treated.

The vicinity of the ground significantly modifies the rotors characteristics. The plots in Fig. 9 show the thrust coefficient, induced velocity, and induced torque coefficient vs h/R. In Fig. 9a the solid symbols are from Ref. 4, which represent flight tests accomplished with different helicopters, whereas the continuous line yields the present results that are obtained by applying the proposed rotor model to a single free rotor. Figure 9a also shows the Cheesman and Bennett results[16] (dot-dashed line), wherein the presence of the ground is modeled by placing under the ground a mirror image that consists of a simple fluid source whose mass flow coincides with that of the rotor. The dashed lines give the data obtained using the Hayden[17] method, which estimates the influence of the ground in hovering through flight-test measurements. According to the literature,[4,5] the Hayden results are found to overpredict the rotor thrust. The figure shows that the present results are in good agreement with the aforementioned flight-test measurements. Figures 9b

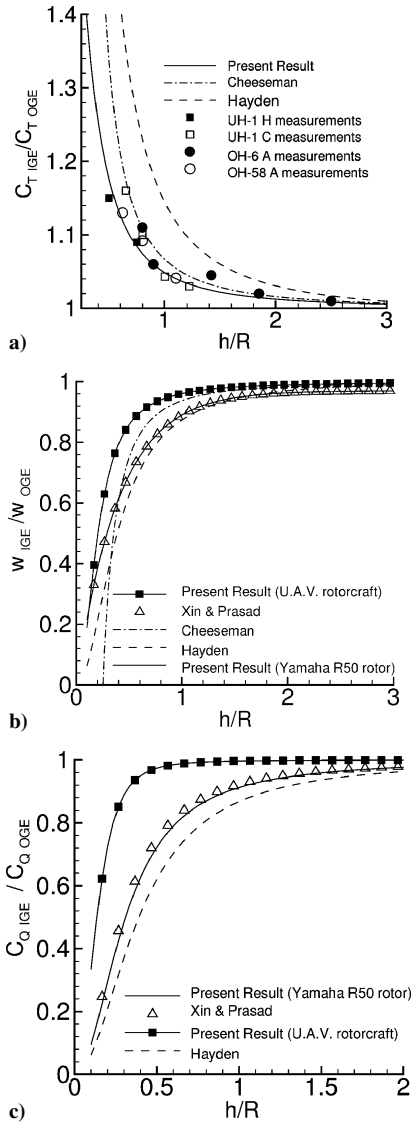

Fig. 9 Rotor in-ground effect.

and 9c compare the induced velocity and the torque coefficient with the other data sources. The solid symbols in Fig. 9b which represent the normalized average inflow in terms of h/R, are from Ref. 12. According to Xin et al.,[12] the continuous line is calculated by applying the proposed model to rotor of the Yamaha R-50, which is a small size, remotely piloted helicopter with a rotor diameter and a rotor speed of 3.07 m and 850 rpm, respectively. The present results, which are compared with Ref. 12 (solid symbols, see figure), show that the rotor model gives results in good agreement with those reported in the literature. The continuous line with the filled symbols provides the data for the UAV here studied.

Also the attitude influences the rotor forces and moments in ground effect. In the diagrams of Figs. 10a–10c, the coefficients C_{Z_T}, C_{X_T}, and C_{m_T} at $V = 0$ are reported as functions of ϑ, where continuous and dashed lines represent the data for shrouded and free rotors, respectively. As well as in the case of the hull, because of the vehicle axial symmetry C_{Z_T} is an even function, while C_{X_T} and C_{m_T} are both odd functions of the pitch angle. While the pitch angle produces minor variations on C_{Z_T}, C_{m_T} exhibits negative slopes whose absolute value increases as h/R tends to zero. This last characteristic is the contribution of the fans system to the vehicle stability in ground effect. The presence of the shroud significantly modifies the thrust force and moment coefficients. In particular a sizable C_{Z_T} increment occurs, which in turn is in agreement with Fig. 8, and an important slope reduction of both C_{X_T} and C_{m_T} is observed, which is caused by the shroud-induced velocity.

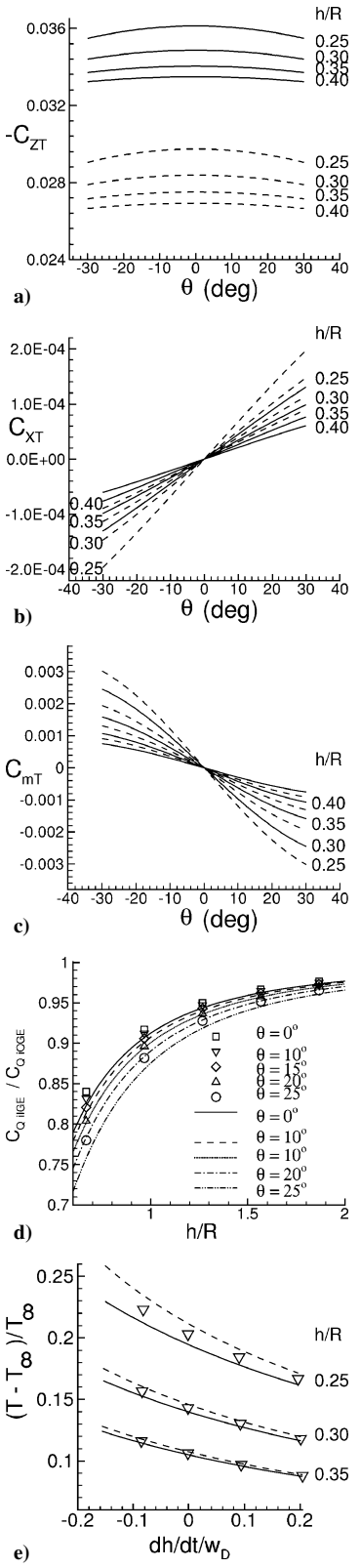

Fig. 10 Influence of height, attitude, and sink rate on the rotors characteristics.

Again, following Ref. 12, the present model is now applied to the Yamaha R-50 rotor (Fig. 10d). The curves give the torque coefficient vs h/R at different ϑ, where the solid symbols are from Ref. 12, while the continuous lines correspond to the present results. According to the literature,[12] for each h/R the vehicle attitude tends to reduce the torque coefficient, and the comparison with Ref. 12 shows that the maximum difference between the two methods is always less than 7%.

Finally, to assess the dynamic ground effect of the rotors system, the thrust variations in term of the dimensionless sink rate are shown in Fig. 10e. Continuous and dashed lines give, respectively, the present model and the results obtained with the unsteady actuator disk theory,[20] whereas the symbols represent the thrust calculated by a code based on the vortex-lattice method,[24] which simulates the dynamic ground effect by means of the mirror image of the actuator disk that moves with a flight-path angle equal to $-\gamma$. These comparisons demonstrates the good agreement between the present data and the results obtained by the actuator disk theory and by the CFD simulations.

Results and Discussion

In this section, to analyze the rotorcraft performance and stability in and out of ground effect, some significant situations that correspond to straight-and-level flight at the trim are studied. Equations (34) are used as equations of motion, and the contribution of the control variables to vehicle dynamics is taken into account through the rotors model. The trim calculation is made by solving a minimization problem with assigned constraints,[25] whereas the vehicle stability is investigated by means of the eigenvalues analysis applied to the linearized motion equations.

Figure 11 depicts some of the significant variables calculated at trim. In Fig. 11a lift and drag coefficients are shown in terms of forward speed. Because of the hull lift cabability caused by the suction force developed by the inlet lip, a sizable nonzero lift coefficient is observed at low velocities, which is about 25% greater than that of the UAV analyzed in Ref. 1. The diagram in Fig. 11b shows the hull trim moment as the function of the flight speed. This is important for the longitudinal stability and controllability because the aerodynamic moment at the trim is balanced by the rotors control moment, generated by longitudinal cyclic pitch. The present results calculated out of ground effect (dashed lines) can be compared with the data from Refs. 1 and 26. In Ref. 1, where a quite similar rotorcraft is studied, the trim moment is a rising function of the forward speed in the speed range $0 \div 30\ \mathrm{m\ s^{-1}}$, and the moments calculated for the velocities of 10 and $20\ \mathrm{m \cdot s^{-1}}$ are about 100 and $180\ \mathrm{N \cdot m}$, respectively. Reference 26 deals with the Cypher, an uninhabited rotorcraft developed by Sikorsky Aircraft Corporation, which is also made by a toroidal fuselage with at the center two coaxial rotors. There, the aerodynamic moment rises to a speed of about $13\ \mathrm{m \cdot s^{-1}}$, where it exhibits its maximum value of about $200\ \mathrm{N \cdot m}$. Although the two vehicles treated in Refs. 1 and 26 exhibit differences with respect to the present one, the corresponding data seem to be somewhat comparable with the results shown in Fig. 11b.

As seen, the ground proximity causes significant variations on the vehicle aerodynamics and on the fans regime in such a way that both aerodynamic and thrust coefficients also vary with height and attitude. This effect is more pronounced at lower h/R. According to the lift reduction for platforms with lifting jet,[10] the fuselage lift capability diminishes as the rotorcraft approaches the ground. The plots in Figs. 11c–11f show the controls expressed in radians in terms of forward speed. For each h/R, the collective pitch δ_C (Fig. 11c) presents a low-speed region, where it remains practically constant until to the speed of about $20\ \mathrm{m \cdot s^{-1}}$, over which it becomes a rising function of V, whereas for what concerns the longitudinal cyclic pitch δ_B (Fig. 11d) its values are directly related to the moment calculated at the trim. For $h/R = 2, 3$, δ_C varies in accordance to the rotors thrust increments, whereas δ_B diminishes until to $20\ \mathrm{m \cdot s^{-1}}$, where reaches its minimum. At higher velocities, according to the hull moment developed at the trim, δ_B rises with V. The calculation made at $h/R = 1$ shows that δ_B is a decreasing function of V in the entire speed range, and for what concerns δ_A and δ_P quite small variations are obtained, but for $h/R < 1$. In this last situation the simultaneous effects of pitch angle and height generate a strong flowfield perturbation on the two rotors in different fashions, which must be balanced by the differential collective pitch. At $h/R = 1$ the peripheral parts of the airframe can touch the ground for certain pitch angles; thus, the trim results are feasible in a more limited speed range. Therefore the corresponding curves are broken at a flight speed less than $24\ \mathrm{m \cdot s^{-1}}$, where $\vartheta \simeq 35$ deg.

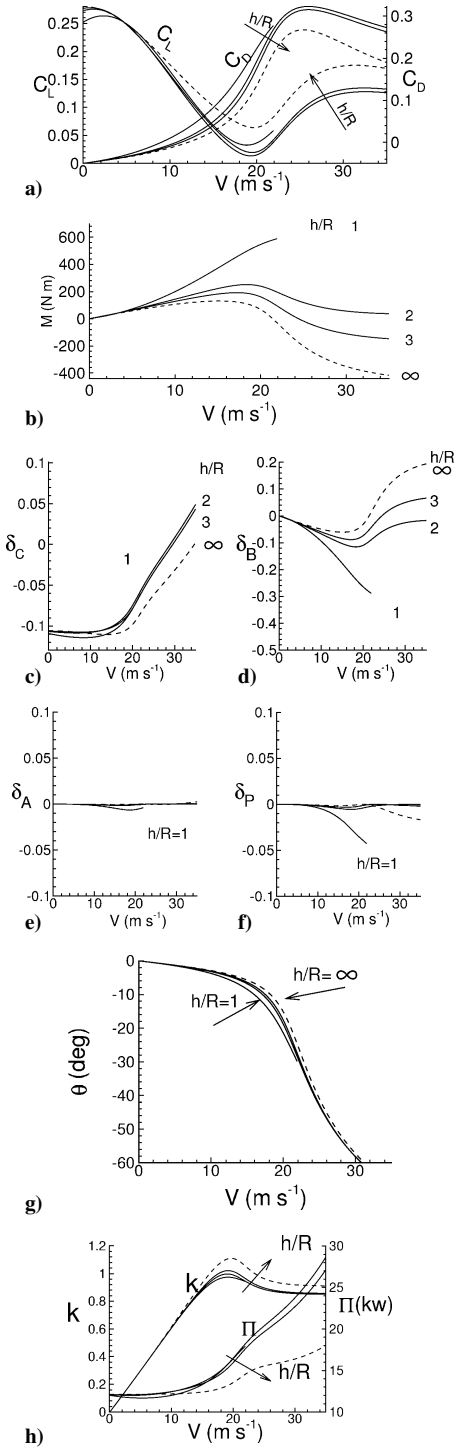

Fig. 11 Trim calculation in horizontal flight at different *h/R*.

For each h/R, the law $\vartheta(V)$ directly depends on the forces calculated at the trim (see Fig. 11g). Because of the smaller variations of lift and drag with respect to the thrust, the pitch angle exhibits relatively small variations as h/R changes. The required power Π_n and the velocity parameter k are represented in Fig. 11h in terms of flight speed. Some comparisons can be made out of ground effect (dashed lines) with the data from Ref. 1. Close the hovering, Π_n is rather similar to that calculated in Ref. 1, whereas for $V \neq 0$ some discrepancies are apparent, which are caused by the different fuselage geometries that develop diverse aerodynamic actions. The higher shroud lift capability than that of the vehicle dealt in Ref. 1 yields smaller required power when $V \neq 0$. The ground effect causes important modifications on Π_n and k. At $h/R = 1$, for $V < 10\ \mathrm{m \cdot s^{-1}}$, a reduction of the 10% of Π_n is observed, whereas at higher velocities, where $\alpha \approx \vartheta \neq 0$, the interaction between the

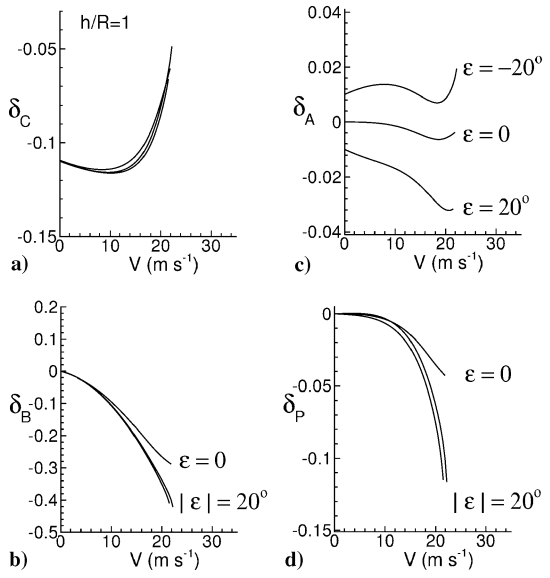

Fig. 12 Trim controls at $h/R = 1$ with inclined ground wall.

rotorcraft and ground generates seeable variations on both aerodynamic and thrust coefficients, which in turn are responsible for the Π_n variations for $V \geq 10\ \mathrm{m \cdot s^{-1}}$. The law $k(V)$ calculated out-of-ground effect (dashed line) is similar in shape to that of Ref. 1, where k is about 10% greater than that here calculated. The downwash reduction from the ground effect causes smaller values of k as h/R approaches zero.

Next, to asses the influence of the ground inclination on the trim, the calculations are repeated in the cases where the ground wall is inclined with respect to the horizon. The wall inclination, which is here obtained by rotating the ground surface of an angle ε around the x axis, is represented by the wall-normal unit vector, that in the inertial frame is given by

$$\boldsymbol{\lambda} = (0, \sin\varepsilon, \cos\varepsilon) \tag{36}$$

To avoid possible touchdown, the trim, whose results are summarized in Fig. 12, is made at $h/R = 1$ for a ground inclination of $\varepsilon = \pm 20$ deg. In such a situation the peripheral parts of the airframe are very close to the wall; thus, the interaction between rotorcraft and ground determines high rotors and fuselage moments that yield not feasible trim for $V \leq 20\ \mathrm{m \cdot s^{-1}}$. Although the state variables result to be rather similar than those just depicted in Fig. 11, the controls are quite different with respect to those obtained for $\varepsilon = 0$. Relevant variations associated with δ_B, δ_A, and δ_P can be observed, especially for what concerns δ_A.

The rotorcraft stability is next evaluated through the eigenvalue analysis applied to the linearized motion equations. The root locus is calculated for various h/R in level flight varying the velocity from 0 to 35 $\mathrm{m \cdot s^{-1}}$ (see Figs. 12a–12d), whereas the several modes are recognized by means of the eigenvector analysis. Figure 13a shows the root locus out of ground effect. According to Ref. 1, at low speed the analysis yields two unstable modes, which are the phugoid (Ph) and the lateral oscillation (L.O.), two aperiodic and stable modes such as the roll (R.S.) and pitch (P.S.) subsidence, and spiral (Sp) and heave (Hv) modes, which are both stable. Because of the vehicle axial symmetry about z_B, the two modes Ph and L.O. degenerate in a single conical mode whose eigenvalues collapse as $V \to 0$. As the flight speed increases, the phugoid eigenvalue diminishes its imaginary part until to intersect the horizontal axis at about 8 $\mathrm{m \cdot s^{-1}}$, where two unstable longitudinal aperiodic modes, that is, A and B (see Fig. 13a), appear. As for L.O. and R.S., the corresponding eigenvalues are approximatively constant until a velocity of about 20 $\mathrm{m \cdot s^{-1}}$, whereas the pitch subsidence P.S. eigenvalue decreases, reaching its minimum at about 20 $\mathrm{m \cdot s^{-1}}$. In the eigenvectors calculated out of ground effect, the Euler angles lag the other state variables, and this is in agreement with the classical flight mechanics, where the Euler angles do not appear in the moment equations of

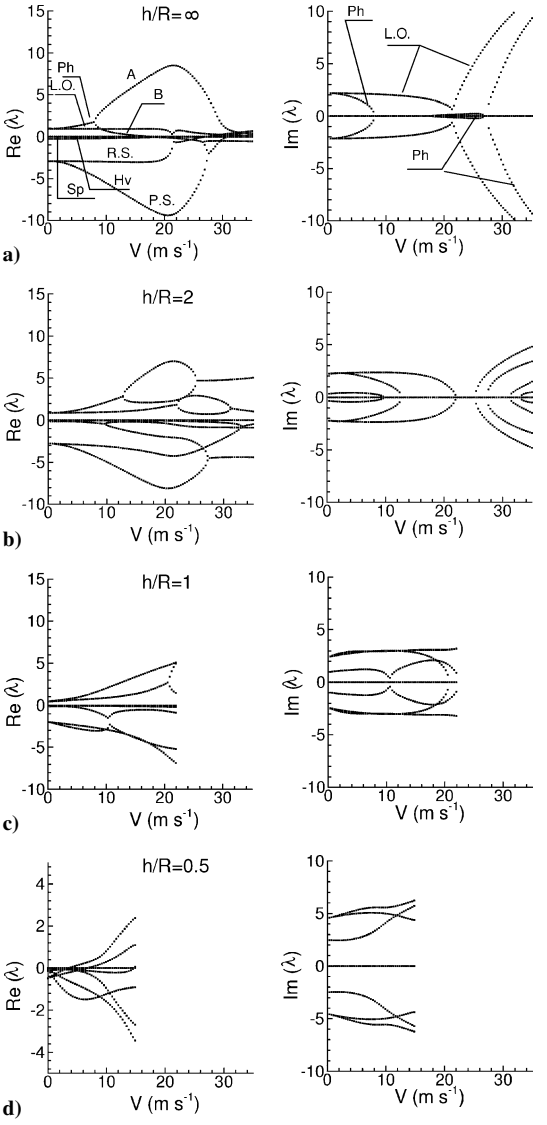

Fig. 13 Root locus in horizontal flight at various h/R.

motion. In ground effect the root locus presents some modifications that become more pronounced as h/R goes to zero. In particular, now, for $h/R \to 0$, the eigenvectors associated with Sp, P.S., and R.S. show Euler angles that do not lag the other state variables. This is a peculiarity of all of the vehicles that fly in proximity of the ground, which is caused by the fact that the right-hand side of the moment motion equations depend on the Euler angles through the aerodynamic coefficients[27] and thrust terms. For an assigned velocity, a significant reduction of the eigenvalues real part is observed for $h/R \to 0$. Because of the hull and rotors moments, under $h/R < 2$ Hv becomes an oscillating and stable mode whose eigenvalue imaginary part increases when h/R goes to zero, whereas the phugoid degenerates in a sort of short-period mode whose stability margin increases when the vehicle approaches the ground. As for the lateral oscillation, it increases its eigenvalue imaginary part and results to be stable for $h/R < 2$. According to the dynamics of the ground-effect machines,[28,29] the eigenvalues-eigenvectors analysis shows that at relatively low velocities, for $h/R \approx 0.5$, all of the modes are stable (see Fig. 13d) because the derivatives $C_{m\theta}$, $C_{mT\theta}$, $C_{l\varphi}$, and $C_{\mathrm{lT}\varphi}$ are negative. Therefore, the Euler angles play a role of paramount importance in the rotorctaft stability in ground effect, especially at low h/R.

Conclusions

This study analyzes the performance and stability of a shrouded-fan UAV by means of two models that determine force and moment developed by the vehicle in the different flight conditions. The

models calculate force and moment developed by the hull and by the rotors and take into account the reciprocal interaction between fuselage and rotors and the ground effect. These features make the main advantage of the proposed method with respect to the other models known in the literature. The limitation of the method is that both the models are based on the potential flow theory where the flow structure about the airframe is in advance assigned and corresponds to the normal working state. The present study shows that the two models give results in good agreement with the various source of data existing in the literature.

The trim analysis in and out of ground effect was accomplished, and the corresponding results were discussed. Out of ground effect the same characteristics just known in the literature are recovered, whereas in ground effect sizable changing in the controls that are caused by the interaction between ground and rotorcraft are observed. The influence of the ground inclination with respect to the horizon is also studied, which is responsible for seeable changing in the controls especially for what concerns the lateral cyclic pitch.

Finally the vehicle stability is analyzed through the eigenvalues-eigenvectors analysis of the linearized motion equations. Whereas the stability out-of-ground effect is somewhat comparable with the data known in the literature, the hull and rotors force and moment, developed in ground effect, cause great modifications in the vehicle stability. According to the classical flight mechanics, the modes calculated out of ground effect exhibit Euler angles that lag the other state variables because such angles do not appear in the right-hand side of the motion equations, whereas in ground effect, because of the incremental force and moment that depend on the Euler angles, the diverse eigenvectors show the Euler angles that do not lag the other state variables. This property, which yields stable modes in ground proximity, is in agreement with the behavior observed in the ground-effect machines.

Acknowledgment

This work was partially supported by Italian Ministry of University.

References

[1]Avanzini, G., D'Angelo, S., and de Matteis, G., "Performance and Stability of a Ducted-Fan Uninhabited Aerial Vehicle," *Journal of Aircraft*, Vol. 40, No. 1, 2003, pp. 86–93.

[2]de Divitiis, N., "Aerodynamic Modeling and Performance Analysis of a Shrouded Fan Unmanned Aerial Vehicle," International Council of the Aeronautical Sciences, Paper 256, Sept. 2002.

[3]Newman, S., *The Foundation of Helicopter Flight*, edited by E. Arnold, 1994, pp. 49–62.

[4]Leishman, J. G., *Principles of Helicopter Aerodynamics*, Cambridge Univ. Press, Cambridge, U.K., 2000.

[5]Kohlman, D. L., *Introduction to V/STOL Airplanes*, Iowa State Univ. Press, Ames, IA, 1981, pp. 45–81.

[6]Padfield, G. D., *Helicopter Flight Dynamics: The Theory and Application of Flying Qualities and Simulation Modeling*, AIAA Education Series, AIAA, Reston, VA, 1996, pp. 1–150.

[7]McCormick, B. W., *Aerodynamics of V/STOL Flight*, Dover, New York, 1999, pp. 231–259, 310–321.

[8]Bramwell, A. R. S., Done, G., and Balmford, D., *Bramwell's Helicopter Dynamics*, 2nd ed., Butterworth Heinemann, Oxford, U.K., 2001, pp. 35–136.

[9]Prouty, R. W., *Helicopter Performance, Stability, and Control*, Krieger, Malabar, FL, 1986, pp. 1–338.

[10]Wyatt, L. A., "Static Test of Ground Effect on Planforms Fitted with a Centrally Located Round Lifting Jet," Ministry of Aviation, CP-749, June 1962.

[11]Levin, B. D., and Wardwell, D. A., "Single Jet-Induced Effect on Small-Scale Hover Data in Ground Effect," *Journal of Aircraft*, Vol. 34, No. 3, 1997, pp. 400–407.

[12]Xin, H., Prasad, J. V. R., Peters, D. A., Itoga, N., Iboshi, N., and Nagashima, T., "Ground Effect Aerodynamics of Lifting Rotors Hovering Above Inclined Ground Plane," AIAA Paper 99-3223, June 1999.

[13]Avanzini, G., and de Matteis, G., "Design of a Shipboard Recovery System for a Shrouded-Fan UAV," International Council of the Aeronautical Sciences, Paper 5.6.3., Sept. 2002.

[14]Xin, H., Prasad, J. V. R., and Peters, D. A., "Unsteady Aerodynamics of Helicopter Rotor Hovering in Dynamic Ground Effect," AIAA Paper 98-4456, Aug. 1998.

[15]Xin, H., Prasad, J. V. R., and Peters, D. A., "Dynamic Inflow Modeling for Simulation of a Helicopter Operating in Ground Effect," AIAA Paper 99-4114, Aug. 1999.

[16]Cheeseman, I. C., and Bennet, W. E., "The Effect of the Ground on a Helicopter Rotor in Forward Flight," Aeronautical Research Council, R & M No. 3021, London, 1957.

[17]Hayden, J. S., "The Effect of the Ground on Helicopter Hovering Power Required," 32nd Annual National V/STOL Forum of the American Helicopter Society, American Helicopter Society, Alexandria, VA, May 1976.

[18]Lamb, H., "On the Motion of Solids Through a Liquid," *Hydrodynamics*, 6th ed., Dover, New York, 1945, pp. 160–201.

[19]Rozhdestvensky, K. V., *Aerodynamics of a Lifting System in Extreme Ground Effect*, Springer-Verlag, Berlin, 2000, pp. 263–318.

[20]Horlock, J. H., *Actuator Disk Theory*, McGraw–Hill, New York, 1978, pp. 12–50.

[21]Etkin, B., *Dynamics of Atmospheric Flight*, Wiley, New York, 1972, pp. 104, 152.

[22]Analytical Methods, Inc., *VSAERO User's Manual*, Rev. E5, April 1994, pp. 1–52.

[23]Kriebel, A. R., "Theoretical Stability Derivatives for a Ducted Propeller," *Journal of Aircraft*, Vol. 1, No. 4, 1964, pp. 203–210.

[24]Lamar, J. E., and Margason, R. J., "Vortex-Lattice FORTRAN Program for Estimating Subsonic Aerodynamic Characteristics of Complex Planforms," NASA-TN-D-6142, L-7262, 1 Feb. 1971.

[25]Stevens, B. L., and Lewis, F. L., *Aircraft Control and Simulation*, Wiley, New York, 1992, pp. 113–195.

[26]Cycon, J. P., "Sikorsky Aircraft UAV Program," *Verflite*, Vol. 38, No. 3, 1992, pp. 26–30.

[27]de Divitiis, N., "Performance and Stability of a Winged Vehicle in Ground Effect," *Journal of Aircraft*, Vol. 42, No. 1, 2005, pp. 148–157.

[28]Walker, N. K., "Influence of Fan and Ducting Characteristics on the Stability of Ground Effect Machines," *Journal of Aircraft*, Vol. 2, No. 1, 1965, pp. 25–32.

[29]Campbell, J. P., *Vertical Takeoff and Landing Aircraft*, MacMillan, New York, 1962, pp. 106, 171.